Science of the Total Environment 658 (2019) 1085–1097

Contents lists available at ScienceDirect

Science of the Total Environment

journal homepage: www.elsevier.com/locate/scitotenv

Impact of intra-annual runoff uniformity and global warming on the thermal regime of a large reservoir

Wei He [a,b], Jijian Lian [b,*], Jian Zhang [a], Xiaodong Yu [a], Sheng Chen [a]

[a] College of Water Conservancy and Hydropower Engineering, Hohai University, Nanjing 210098, China
[b] State Key Laboratory of Hydraulic Engineering Simulation and Safety, Tianjin University, Tianjin 300072, China

HIGHLIGHTS

- Intra-annual runoff uniformity tends to decrease in natural basins of South China.
- Lower runoff uniformity increases water temperature and decreases thermal stability
- Global warming increases both water temperature and thermal stability.
- Global warming has a greater influence than intra-annual runoff uniformity.
- Effects of two methods aimed at controlling the thermal regime were analyzed.

GRAPHICAL ABSTRACT

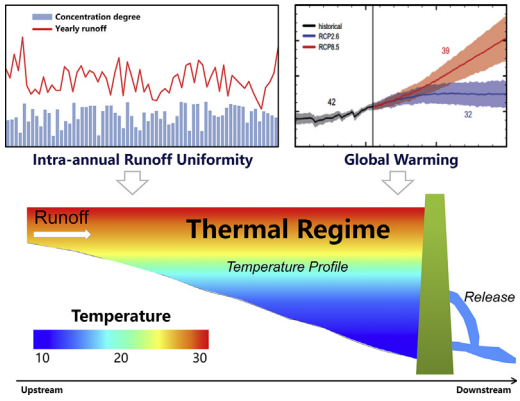

ARTICLE INFO

Article history:
Received 17 September 2018
Received in revised form 30 November 2018
Accepted 13 December 2018
Available online 17 December 2018

Editor: Ralf Ludwig

Keywords:
Intra-annual runoff uniformity
Global warming
Thermal regime
Sanbanxi reservoir
CE-QUAL-W2

ABSTRACT

Thermal stratification is common in reservoirs and greatly influences the aquatic environment. Changes in the uniformity of intra-annual runoff have been detected in several basins, but few studies have focused on the impacts that these changes have on thermal regimes. Using runoff data for Sanbanxi Reservoir, China, during 1950–2015, the long-term trends of intra-annual runoff uniformity were statistically analyzed and extrapolated for the 2050s and 2090s, and the relationship between these trends and the thermal regime of the reservoir were investigated. Moreover, the thermal regime was evaluated for future climate scenarios accounting for global warming. This study shows the following: 1) for South China, the concentration degree (C_d) for the distribution of intra-annual runoff in natural basins such as Sanbanxi Reservoir tended to be higher, but for rivers significantly impacted by human activities, C_d tended to be lower. 2) a higher C_d was associated with an increased reservoir temperature and released water temperature, and decreased thermal stability. For Sanbanxi Reservoir, a 10% increase in C_d corresponded to a change in annual average temperature, thermal stability, and released water temperature of 0.036 °C, −48.4 J m^{-2}, and 0.153 °C, respectively. These changes were larger in summer than in other seasons; 3) global warming is predicted to increase reservoir temperature, released water temperature, and thermal stability, having a more significant influence on these parameters than intra-annual runoff uniformity; 4) future changes in thermal regimes will intensify oxygen stratification and hypolimnetic anoxia, promoting algal blooms, and delaying fish spawning. Effects of two methods aimed at controlling the thermal regime were also analyzed, including changing the operation level and intake elevation of the reservoir. This study investigated the response of the thermal regime of Sanbanxi Reservoir to climate change, and provides theoretical support for the management of water temperature and the reservoir's aquatic environment.

© 2018 Published by Elsevier B.V.

* Corresponding author.
E-mail address: jjlian@tju.edu.cn (J. Lian).

https://doi.org/10.1016/j.scitotenv.2018.12.207
0048-9697/© 2018 Published by Elsevier B.V.

1. Introduction

The combination of the impoundment of water and solar radiation frequently leads to thermal stratification in reservoirs. The water column is usually thermally stratified during spring, summer, and autumn, with a warmer surface layer (the epilimnion), a colder bottom layer (the hypolimnion), and a transient layer between the two (the metalimnion) (Milstein and Zoran, 2001; Saber et al., 2018). Thermal stratification of a water body significantly influences water quality, the behavior of aquatic life and water irrigation (Elçi, 2008; Huang et al., 2014; Wang et al., 2014; Yang et al., 2015; Zouabi-Aloui et al., 2015; Zhu et al., 2013). Stronger stratification increases physical stability of the water column, and reduces vertical exchange and mixing (Anohin et al., 2006; Wu et al., 2016). As a result of weak water exchange and mixing and a lack of light for photosynthesis, hypolimnetic dissolved oxygen is typically depleted, and water quality and fish biomass are reduced (Elçi, 2008; Hetherington et al., 2015; Milstein and Zoran, 2001; Prats et al., 2018; Zhang et al., 2015). Additionally, owing to thermal stratification and low water intake, the released water temperature usually differs from the natural inflow temperature, which can be harmful for downstream habitats (He et al., 2018; Soleimani et al., 2016; Zouabi-Aloui et al., 2015). Many hydrological and meteorological factors can influence reservoir thermal regimes, including the discharge and temperature of inflow runoff, mode of reservoir operation, air temperature, and solar radiation (Butcher et al., 2015; Han et al., 2000; Liu et al., 2011; Saber et al., 2018; Soleimani et al., 2016). Among these factors, thermal regimes are sensitive to runoff discharge, which can impact hydrodynamic circulation, stratification duration, and thermocline thickness (Butcher et al., 2015; Han et al., 2000; Liu et al., 2011). High input from runoff significantly promotes the mixing of stratified water and consequently disturbs the stratification (Huang et al., 2014; Wang et al., 2012).

Alongside climate change and human activities, changes in runoff have been detected in many basins. Firstly, increases and decreases in runoff magnitude, such as the yearly mean runoff discharge, have been observed in the Tarim, Dongjiang, and Hun–Tai rivers. Anthropogenic and climate change effects have also been identified, including changes in precipitation and evapotranspiration, vegetation type and soil hydraulic properties, agricultural irrigation, and discharge diversion (Lin et al., 2017; Petersen et al., 2012; Xu et al., 2008; Zhang et al., 2011). Secondly, changes in intra-annual runoff uniformity have been observed in some rivers, including the Yangtze, Yalong, Dongjiang, and Songhua Rivers in China, the Vermillon River in Canada, the Alpine catchments in Italy and many rivers in northwest USA, which may be due to upstream regulation of hydraulic projects or alterations in rainfall and snowmelt (Assani et al., 2010; Bocchiola, 2014; Li et al., 2014; Luce and Holden, 2009; Wang et al., 2015; Xie et al., 2011; Zhao et al., 2012). The impact of variations in runoff magnitudes on the thermal regimes of reservoirs has also been studied (Huang et al., 2014; Wang et al., 2012), but the potential impact of intra-annual runoff uniformity (i.e. the degree of uniformity in the distribution of runoff during the year) on the thermal characteristics of river basins has not yet been investigated.

According to the IPCC (2013), global warming is an unequivocal factor in climate change, and many of its observed impacts are unprecedented over decades to millennia. Researchers have statistically and/or numerically studied the potential influence of global warming on the thermal dynamics of reservoirs, and have shown that global warming increases water temperature, thickens the thermocline, and extends the duration of stratification (Modiri-Gharehveran et al., 2014; Prats et al., 2018; Zhang et al., 2015). However, existing evaluations of thermal regimes predominantly consider the impact of global warming while studies on the impact of other changes, such as hydrological alterations, are rare.

Sanbanxi Reservoir is a deep reservoir with strong thermal stratification, and its thermal regime is critical to the ecology of the reservoir area and its downstream reaches. According to the previously recorded data, runoff discharge seems to be increasing during the flood season but is decreasing during the dry season, and the thermal effect of this phenomenon is yet to be evaluated. Therefore, this study aims to statistically estimate the trend of intra-annual runoff uniformity using observational data, and analyze the associated impacts on the thermal regime, while also accounting for global warming.

This study is structured as follows: in Section 2, the study site, evaluation method for runoff, setup, calibration, and validation of numerical models, and model scenarios are described. Section 3 presents the results including patterns of intra-annual runoff uniformity and thermal regimes under different climate conditions. Section 4 provides an extended discussion, and conclusions are presented in Section 5.

2. Materials and methods

2.1. Study site

The study site was Sanbanxi Reservoir, a large reservoir located in Southwest China (26.4–26.7°N, 108.5–109.1°E) (Fig. 1). The reservoir has a total capacity and maximum water depth of approximately 4.09 billion m^3 and 160 m, respectively, and the operational parameters are described in He et al. (2018). Because of the significant water depth and scarce occurrence of floods in recent years, thermal stratification often exists in the reservoir, which has a significant influence on the basin environment and ecology (Ou et al., 2014).

2.2. Evaluation of runoff and global warming

2.2.1. Evaluation of inflow runoff

A trend analysis was conducted using monthly average runoff for the period 1950–2015 (66 years). The annual average runoff ($\overline{q}$) was used to describe the runoff magnitude, and the commonly used concentration degree (C_d) and concentration period (C_p) were used to estimate the intra-annual runoff distribution (Li et al., 2010; Tu et al., 2015; Xie et al., 2005; Zhang and Qian, 2003). Calculation of C_d and C_p is based on the monthly runoff discharge vector. C_d represents the degree to which yearly runoff concentrates within 12 months. It is a dimensionless number ranging from 0 to 1: a larger value indicates that a higher percentage of the annual runoff occurred during the main flood season. C_p represents the period (month) in which the runoff is concentrated, and values of 0, 30°, 60°, …, 300°, and 330° correspond to January, February, March, …, November, and December, respectively. For a runoff discharge time series, C_d and C_p are defined as follows:

$$C_{di} = \sqrt{R_{xi}^2 + R_{yi}^2}/R_i \tag{1}$$

$$C_{pi} = \arctan\left(R_{xi}/R_{yi}\right) \tag{2}$$

$$R_i = \sum_{j=1}^{n} q_{ij} \tag{3}$$

$$R_{xi} = \sum_{j=1}^{n} q_{ij}\, sin\theta_j \tag{4}$$

$$R_{yi} = \sum_{j=1}^{n} q_{ij}\, \cos\theta_j \tag{5}$$

where i is the year (i = 1950, 1951, …, 2015, covering the 66 years included in this study); j is the month ($j = 1, 2, 3, \ldots, 12$); q_{ij} is the monthly average runoff in the jth month of ith year; and θ_j is the azimuth of the jth month (θ = 0, 30, 60, …, 300, 330°); R_i, R_{xi} and R_{yi} are intermediate variables.

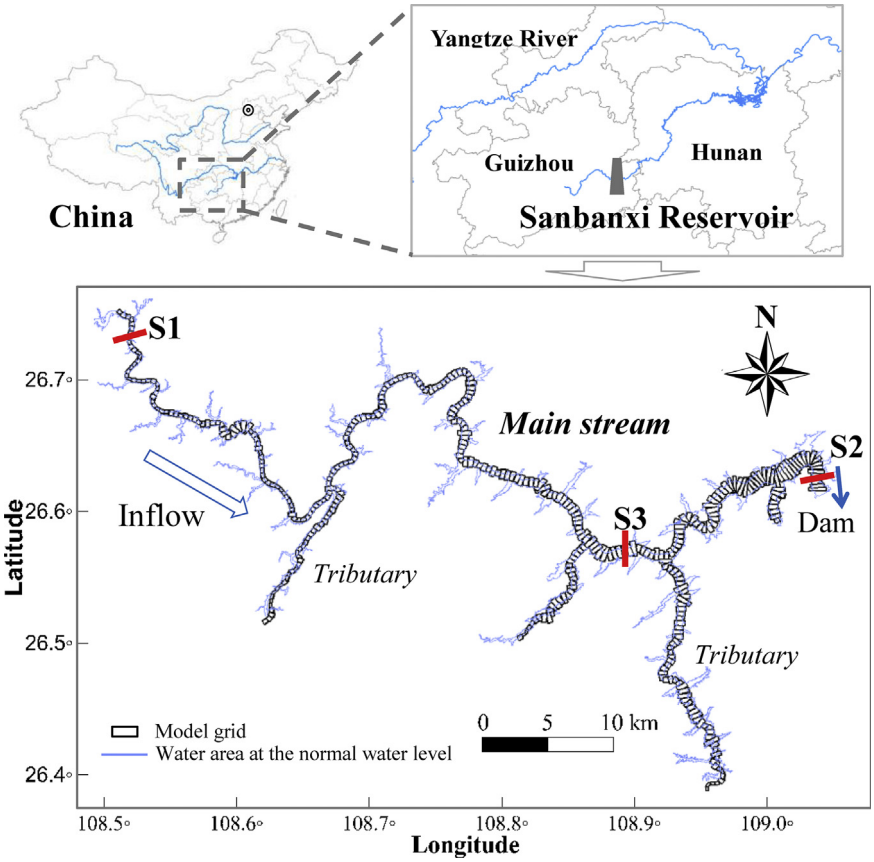

Fig. 1. Plan view and model grid of the study site. S1 and S2 are monitoring sections at the tail and 1.1 km upstream of the dam respectively. S3 is the representative section 25 km upstream of the dam.

2.2.2. Trend analysis

The non-parametric Mann–Kendall (MK) test was introduced to determine the significance of the trend (Assani et al., 2010; Bocchiola, 2014; Lin et al., 2017; Zhang et al., 2011), and the Theil-Sen estimator (β) was introduced to quantify the magnitude of the long-term trend (Li et al., 2014; Gu et al., 2016; Stahl et al., 2010; Sun et al., 2015); these two methods have been extensively applied in trend analysis of river runoff, covering basins in China, Canada, Italy, France, and many other European countries.

In the original MK test, for a time series, the normalized statistical index UF_k is calculated under the null hypothesis (H_0) that there is no change. An increasing (or decreasing) trend is detected if $UF_k > 0$ (<0). In the two-tailed test, when UF_k falls outside the confidence interval (generally $a = 0.05$), H_0 is rejected, demonstrating a significant trend, and vice versa. Moreover, before the original MK test, to avoid serial correlation, a "pre-whiten" process is conducted on the time series by eliminating the lag-1 serial correlation (r_1) (Li et al., 2014; Zhang et al., 2011).

The time series was regarded as a linear trend with noise, and the Theil-Sen estimator (β) can be used to determine the variation in the slope of a hydrological or meteorological time series x_i ($i = 1, 2, \cdots, n$):

$$\beta = Median\left(\frac{x_j - x_i}{j - i}\right) \qquad \forall 1<i<j<n \tag{6}$$

An increasing (or decreasing) trend is detected if $\beta > 0$ (<0), and a larger value of $|\beta|$ indicates a more significant increasing or decreasing trend.

2.2.3. Magnitude of global warming

According to the IPCC (2013), there are four typical emission scenarios for global warming: RCP2.6, RCP4.5, RCP6.0, and RCP8.5. The increase in mean air temperatures at Sanbanxi Reservoir for the periods 2046–2065 and 2081–2100 relative to 1986–2005 are shown in Table 1. In terms of seasonality, the 50% percentile relative air temperature changes in the RCP4.5 scenario for both June to August and October to March during 2046–2065 (2081–2100), relative to 1986–2005, are both in the range of 1.5–2 °C (2–3 °C). For simplicity, a seasonally constant increase in air temperature is considered here in future climate scenarios.

2.3. 2-D hydrodynamic and temperature numerical model

2.3.1. Model setup

The laterally averaged, two-dimensional, and open-source CE-QUAL-W2 was used to setup a hydrodynamic and temperature model covering the main stream and large tributaries, as shown in Fig. 1. CE-QUAL-W2 is applicable to relatively elongated and deep water bodies, and has been validated in hydrodynamic and temperature simulations covering the Three Gorges Reservoir in China, Lake Spaulding in the

Table 1
Increase in air temperature at Sanbanxi Reservoir under future scenarios (°C).

Emission scenarios	Mean (°C)		Likely range (°C)	
	2046–2065	2081–2100	2046–2055	2081–2100
RCP2.6	1.25	1.25	1–1.5	1–1.5
RCP4.5	1.75	2.5	1.5–2	2–3
RCP6.0	1.75	2.5	1.5–2	2–3
RCP8.5	2.5	4.5	2–3	4–5

USA and Sejnane Reservoir in Tunisia (Cole and Wells, 2015; Lian et al., 2014; Ma et al., 2015; Zouabi-Aloui et al., 2015). The basic equations for the model are shown in Appendix 2. Sanbanxi Reservoir was represented as 419 longitudinal segments with lengths of 100–390 m and 100 vertical layers with thicknesses of 2 m according to the topographic data recorded in 2014 with an accuracy of 30 m. The W2 turbulence closure algorithm was used. There is only one inflow entrance upstream of the main stream (S1 in Fig. 1) and there are no other inflow entrances from the tributaries. The boundary data were input with a daily resolution, including inflow discharge and temperature, released discharge, air temperature, solar radiation, wind speed and direction, precipitation and evaporation, and cloud cover. The precipitation temperature was set equal to the air temperature.

2.3.2. Model calibration and validation

In the numerical model, the wind sheltering coefficient and sediment temperature were determined according to the geography and land features, and the Manning coefficient, longitudinal eddy viscosity, longitudinal eddy diffusivity, fraction absorbed at the water surface and extinction coefficient were calibrated with reference to the adjacent Three Gorges Reservoir (Lian et al., 2014; Ma et al., 2015) and other reservoirs (Cole and Wells, 2015; Zouabi-Aloui et al., 2015). The mean absolute error (MAE), root mean square error (RMSE), and mean absolute relative error (MARE), were used to quantify bias and goodness of fit (Lian et al., 2015; Ma et al., 2015; Modiri-Gharehveran et al., 2014; Moriasi et al., 2007), as expressed below.

$$\mathrm{MAE} = \frac{1}{n}\sum_{i=1}^{n}\left|Y_i^{obs} - Y_i^{sim}\right| \tag{7}$$

$$\mathrm{RMSE} = \sqrt{\frac{1}{n}\sum_{i=1}^{n}\left(Y_i^{obs} - Y_i^{sim}\right)^2} \tag{8}$$

$$\mathrm{MARE} = \frac{1}{n}\sum_{i=1}^{n}\frac{\left|Y_i^{obs} - Y_i^{sim}\right|}{Y_i^{obs}} \times 100\% \tag{9}$$

where

n is the number of observations; Y_i^{obs} is the ith observation; Y_i^{sim} is the ith simulated value; Y^{mean} is the mean of observations.

The 2-D model was calibrated using observational data from January 2013 to April 2014. Daily hydrological and meteorological data were input, and the calculated values of water level, temperature profile of S2 (Fig.1), and released water temperature were compared with measured values, as shown in Table 2 and in the left panel of Fig. 2. As can be seen, calculated water levels had a good fit. For the temperature profiles, the MAE and RMSE values were all below 1.2 and 1.8 °C, respectively, and MARE values for the depths 0.5, 10, 30 and 50 m were <8%. This error may have been due to the adoption of daily hydrological and meteorological data, which ignore their hourly variations. For the calibration of the released water temperature, the MAE, RMSE and MARE values were 0.50 °C, 0.65 °C and 2.8%, respectively.

The model was validated using observational data from October 2015 to December 2015, and the validation results are shown in the right panel of Fig. 2. The MAE, RMSE and MARE values were all below 0.35, 0.50 and 3%, respectively. Allowing for multiple factors influencing the thermal regime of a large and deep reservoir, the model performance was satisfactory, and the model considered to simulate the spatial–temporal temperature distribution well.

2.4. Model scenarios

The model scenarios were set according to the results of the runoff trend analysis (described in Section 3.1): the $\overline{q}$ and C_p did not show significant long-term changes, while C_d showed a significant increasing trend, reaching approximately 0.465 (+13%) and 0.518 (+26%) in the years 2046–2065 and 2081–2100, respectively. As C_d increased, the monthly runoff increases from May to August and decreased in other months, as shown in Fig. 3. In addition, global warming was taken into account to evaluate the thermal regime, including the RCP4.5 medium–low emission scenario and the RCP8.5 high emission scenario. Global warming primarily influenced the air and inflow temperatures, as shown in Table 3. Scenarios A0, A1, and A2 were used to study the one-sided impact of the intra-annual runoff uniformity, and scenarios A3 to A6 were used to evaluate the thermal regime accounting for global warming.

Table 2
Principal parameters for the numerical model.

Model parameter	Adopted value
Bottom manning coefficient (s $m^{-1/3}$)	0.035
Longitudinal eddy viscosity (m^2 s^{-1})	1[a,b]
Longitudinal eddy diffusivity (m^2 s^{-1})	0.4[a]
Coefficient of bottom heat exchange (W m^{-2} s^{-1})	0.3[a]
Fraction absorbed at the water surface	0.45[a,c]
Extinction coefficient (m^{-1})	0.45[a,c,d]

[a] Cole and Wells (2015).
[b] Lian et al. (2014).
[c] Ma et al. (2015).
[d] Zouabi-Aloui et al. (2015).

The initial conditions were set using the measured water level and temperature profile on March 15, 2014. To limit the influence of the initial conditions (Prats et al., 2018), the simulation contained five dispatching periods. The results of the last dispatching period were extracted to analyze the thermal regime. In addition, a cumulative impact analysis was performed and showed that the simulation results of the 3rd–5th dispatching periods were largely the same, indicating that the initial conditions did not have a significant influence on the results. The operation water levels for all scenarios were set based on the normal regulation scheme, and the released discharge was derived according to the inflow and water level capacity curve. For the baseline conditions, hydrological and meteorological boundary values for the 15th of each month were taken from historical monthly mean values during the period 1950–2015, and boundary values for other days were linearly interpolated. In the 2050s and 2090s, increases in air temperature were derived according to the IPCC (2013), and the increase in the inflow temperature was calculated using historic data (Table 3 and Appendix 3). In addition, monthly means of the metrological boundary conditions including air temperature, solar radiation, wind speed and direction, precipitation and evaporation, and cloud cover for the period 1951–2001 were used. In addition, the dimensionless Lake Number showed that the impact of wind on the Sanbanxi Reservoir thermal regime was small. Based on observational data from January 2013 to April 2014, the yearly mean value of Lake Number was 7.1, and the calculated monthly mean values were above 3, except for February and March, indicating that the upwelling of the hypolimnetic column caused by wind stress was unapparent (Anohin et al., 2006). In February and March, the thermal stratification was relatively weak with a vertical temperature gradient of ~0.035 °C·m^{-1}, and the effect of upwelling on the vertical temperature profile was also limited.

2.5. Evaluation of thermal regime

2.5.1. Spatial–temporal distribution of the reservoir temperature

As the temperature profile was generally uniform along the reservoir area, the vertical temperature distribution 25 km upstream of the dam (S3 in Fig. 1) was considered as the representative section to quantitatively analyze the temperature profile. The volume-weighted average water temperature at depths of 0–20, 20–50, 50–90, and >90 m was recorded, and the volume-weighted average temperature of the whole reservoir was calculated. Additionally, the released water temperature was also obtained via numerical simulation.

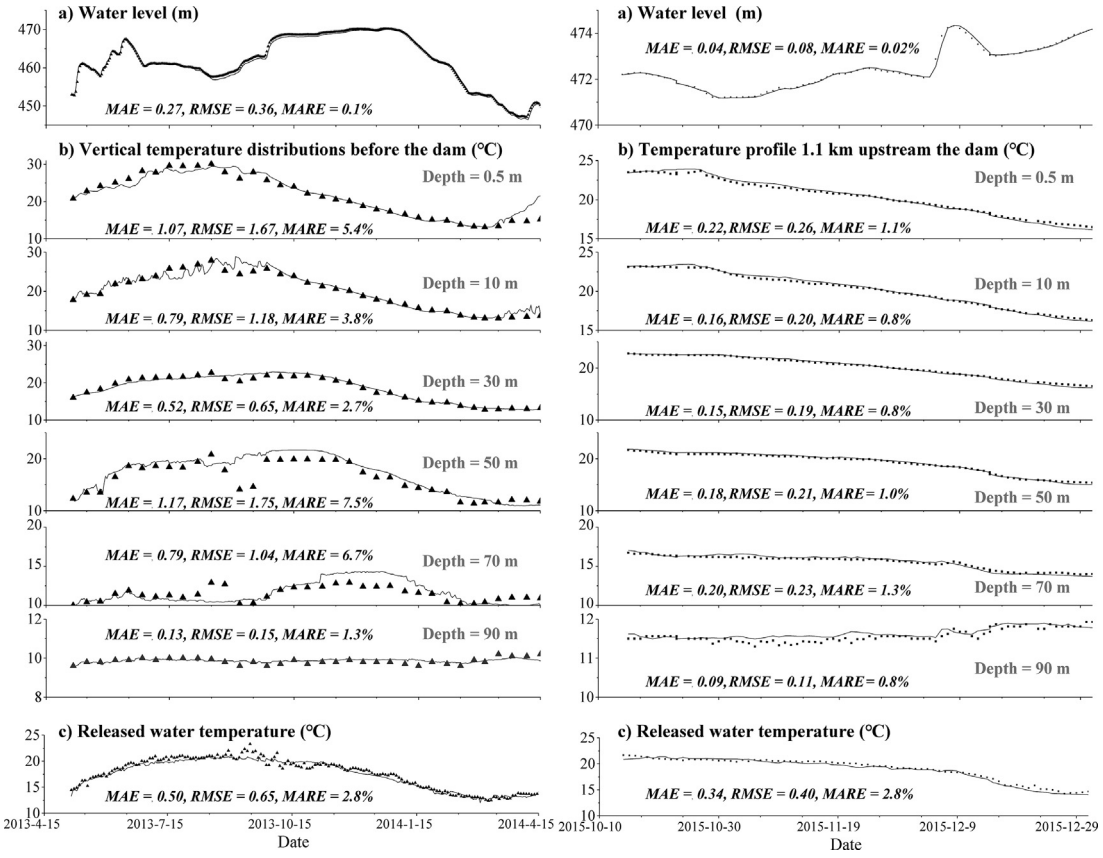
a) Water level (m)
MAE = 0.27, RMSE = 0.36, MARE = 0.1%
b) Vertical temperature distributions before the dam (°C)
Depth = 0.5 m
MAE = 1.07, RMSE = 1.67, MARE = 5.4%
Depth = 10 m
MAE = 0.79, RMSE = 1.18, MARE = 3.8%
Depth = 30 m
MAE = 0.52, RMSE = 0.65, MARE = 2.7%
Depth = 50 m
MAE = 1.17, RMSE = 1.75, MARE = 7.5%
MAE = 0.79, RMSE = 1.04, MARE = 6.7%
Depth = 70 m
MAE = 0.13, RMSE = 0.15, MARE = 1.3%
Depth = 90 m
c) Released water temperature (°C)
MAE = 0.50, RMSE = 0.65, MARE = 2.8%
2013-4-15
2013-7-15
2013-10-15
2014-1-15
2014-4-15
Date
a) Water level (m)
MAE = 0.04, RMSE = 0.08, MARE = 0.02%
b) Temperature profile 1.1 km upstream the dam (°C)
Depth = 0.5 m
MAE = 0.22, RMSE = 0.26, MARE = 1.1%
Depth = 10 m
MAE = 0.16, RMSE = 0.20, MARE = 0.8%
MAE = 0.15, RMSE = 0.19, MARE = 0.8%
Depth = 30 m
MAE = 0.18, RMSE = 0.21, MARE = 1.0%
Depth = 50 m
MAE = 0.20, RMSE = 0.23, MARE = 1.3%
Depth = 70 m
MAE = 0.09, RMSE = 0.11, MARE = 0.8%
Depth = 90 m
c) Released water temperature (°C)
MAE = 0.34, RMSE = 0.40, MARE = 2.8%
2015-10-10
2015-10-30
2015-11-19
2015-12-9
2015-12-29
Date

Fig. 2. Calibration (left panel) and validation (right panel) results of the numerical simulation. The solid lines are the calculated values and the points are the measured values.

2.5.2. Thermal stability

The Schmidt stability (S_t) was used to determine the stratification strength and physical stability of a reservoir (Butcher et al., 2015; Wang et al., 2012; Wu et al., 2016). S_t (J m^{-2}) is zero in an isothermal reservoir, and larger values demonstrate stronger stratification, as expressed below:

$$S_t = \frac{g}{A_0}\int_{Z_0}^{Z_m} A_z(z-z^*)(\rho_z-\rho^*)dz \tag{10}$$

where g is the gravitational acceleration, m s^{-2}; A_0 is the surface area of the reservoir, m^2; z is the water depth, m; A_z is the water area at depth z, m^2; ρ_z is the density at depth z, kg m^{-3}; ρ^* is the volume-weighted average water density of reservoir, kg m^{-3}; and z^* is the depth of mean density, m.

2.5.3. Stratification duration

Vertical mixing and exchange within a water column are restricted under a significant vertical temperature gradient, and a longer stratification duration limits improvements in water quality (Wang et al., 2012; Lee et al., 2012). Due to a lack of a uniform threshold to define a thermocline, the commonly used 0.2 °C m^{-1} for reservoirs and the continental shelf was adopted here (Zhang et al., 2015).

3. Results

3.1. Runoff trend analysis

Using observational runoff data for the period 1950–2015, the trend analyses for $\overline{q}$, C_p, and C_d are shown in Fig. 4. The lag-1 serial correlation (r_1) values of $\overline{q}$, C_p, and C_d are 0.175,–0.018, and −0.127, respectively, which are in the range of [$r_{a=-0.05} = -0.26$, $r_{a=+0.05} = 0.23$]. These time series are judged to be independent at the 0.05 significance level,

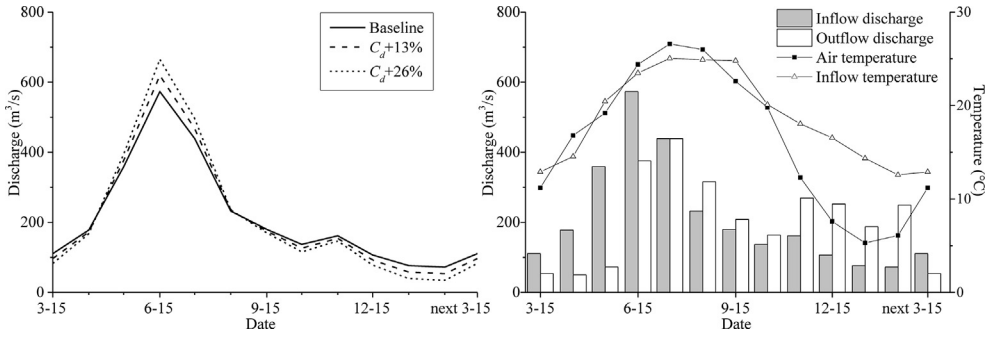

Fig. 3. Different intra-annual runoff uniformities and boundary conditions during a dispatching period.

Table 3
Model scenarios for intra-annual runoff uniformities and global warming.

Number	Description		Concentration degree (C_d)	Temperature increase (°C)	
				T_{air}	T_{inflow}
A0	Baseline		0.411	0	0
A1	Change in C_d		0.465 (+13%)	0	0
A2			0.518 (+26%)	0	0
A3	The 2050s:	RCP4.5	0.465 (+13%)	1.75	1.16
A4	change in C_d and T_{air}	RCP8.5		2.5	1.65
A5	The 2090s:	RCP4.5	0.518 (+26%)	2.5	1.65
A6	change in C_d and T_{air}	RCP8.5		4.5	2.97

and the original MK test was conducted. The UF_k curves for $\overline{q}$ and C_p remain within the ±0.05 significance level, and do not show significant long-term increasing or decreasing trends. The mean value of C_p is 156°, indicating that the runoff levels are concentrated around June. The UF_k curve for C_d exceeds the +0.05 significance level near the year 2007, and C_d shows a significant long-term increasing trend.

The Theil-Sen estimators (β) for $\overline{q}$, C_p, and C_d are −0.302 $m^3\ s^{-1}\ a^{-1}$, 0.233 a^{-1}, and 0.0013 a^{-1}, respectively. Using measured runoff for the period of 2007–2015, when the reservoir was impounded, the monthly mean of the inflow discharge is calculated, and the average concentration degree (C_d) is 0.411. Assuming that $\overline{q}$ and C_p are unchanged, C_d for the years 2046–2065 (~40 years later) and 2081–2100 (~80 years later) is predicted to reach approximately 0.465 (+13%) and 0.518 (+26%), respectively.

3.2. Impact of intra-annual runoff uniformity

3.2.1. Water temperature

Through numerical simulations, the average water temperatures of different layers were obtained, as shown in Fig. 5a. As C_d increases, more warm water enters the reservoir in summer and less cold water enters in winter, and the water temperature consequently increases. As C_d increases by 13% and 26%, the volume-weighted average temperature of the inflow increases by 0.28 °C and 0.56 °C, respectively, compared with the baseline (21.13 °C), and the annual average temperature of the whole reservoir increases by 0.05 °C and 0.09 °C, respectively. The average temperatures for the depths 0–20, 20–50, 50–90, and >90 m increases by 0.02, 0.08, 0.06, and 0 °C (0.04, 0.16, 0.12, 0.01 °C), respectively. Because the inflow temperature lies between the hypolimnetic and epilimnetic temperatures, the majority of the inflow runoff enters the reservoir at depths of 20–50 m and 50–90 m. Therefore, as C_d increases, the water column is more significantly affected at depths of 20–50 m and 50–90 m than the hypolimnion and epilimnion. Because air temperature and solar radiation are not affected by different C_d values, the change in the epilimnetic temperature is small. Owing to thermal stratification, the hypolimnion is relatively unaffected by the inflow runoff, and the hypolimnetic temperature hardly changes. In general, as C_d increases, the temperatures of the whole reservoir and its middle layers increase, and the hypolimnetic and epilimnetic temperatures hardly change.

3.2.2. Stratification duration

In spring, the warm inflow enters the reservoir and elevates the epilimnetic temperature, establishing temperature gradient above 0.2 °C m^{-1} at a depth of around 10 m below the water surface. In summer, because of the hot air and inflow, a significant temperature gradient continuously exists at a depth of around 10 m. Moreover, as water temperature rises, the temperature gradient at a depth of around 60 m gradually exceeds 0.2 °C m^{-1}. In autumn and winter, because the air and inflow temperatures decrease, the water column in the epiliminion and metaliminion successively cools. The thermocline at a depth of around 10 m diminishes in late September, and the thermocline at a

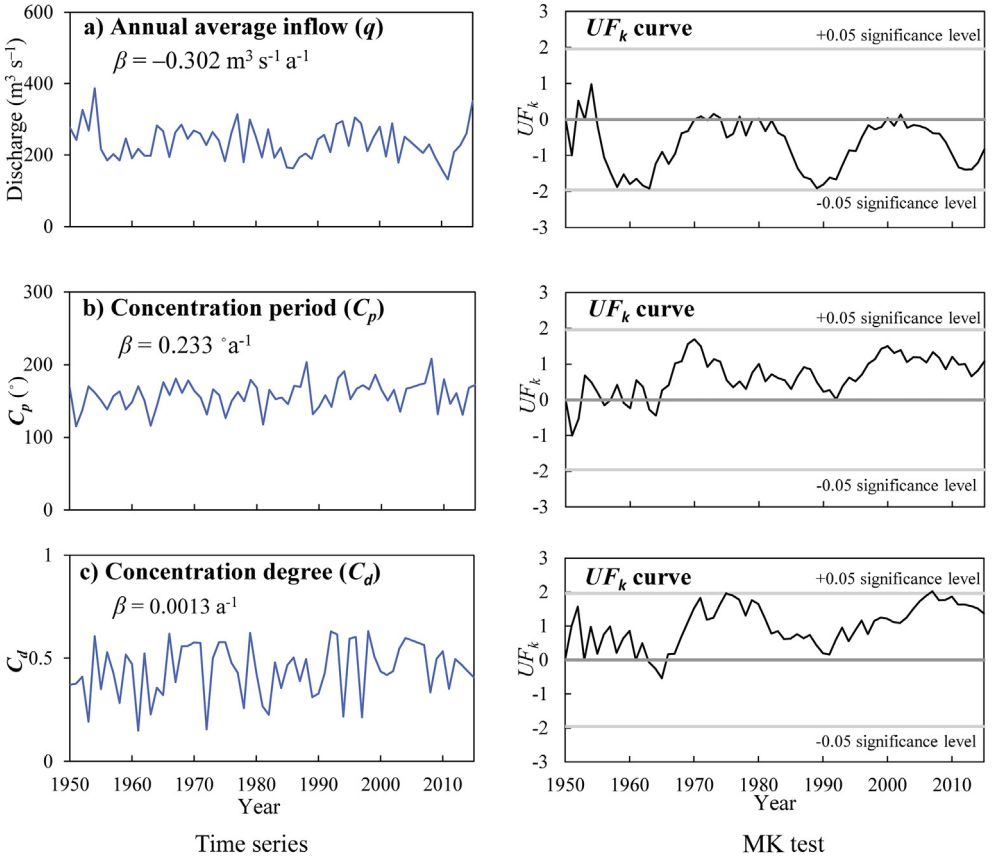

Fig. 4. Time series and MK tests for $\overline{q}$, C_p, and C_d.

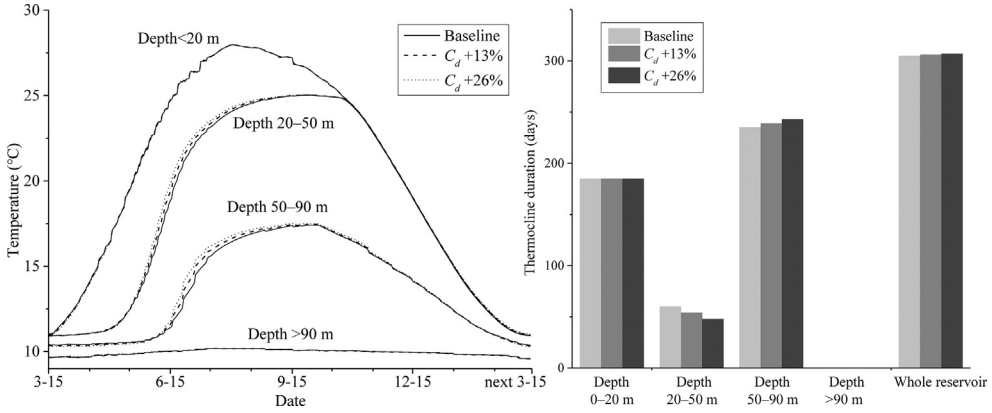

Fig. 5. Water temperatures and stratification durations of different water layers over one year.

depth of around 60 m diminishes in December. In general, the stratification duration at a depth of 50–90 m is ~8 months ranging from June to the following January, and is larger than that at a depth of 0–20 m (~6 months, April–September) and a depth 20–50 m (~2 months, April–May).

As C_d increases, the water temperature of the metalimnion increases, affecting the stratification duration, as shown in the right panel of Fig. 5b. The temperature increases at depths of 20–50 m, approaching the epilimnetic temperature. The temperature gradient and stratification duration decrease. Conversely, the temperature at depths of 50–90 m increases, diverging significantly from the hypolimnetic temperature, and the corresponding stratification duration increases. Across all the water layers, the stratification duration increases slightly.

3.2.3. Thermal stability

The annual thermal stability variations are shown in Fig. 6. As C_d increases, S_t decreases in summer and increases in winter. In summer, firstly, the inflow discharge increases and promotes vertical water mixing. Secondly, the thermal stability is related to the dispersion degree of the temperature. More warm water enters the reservoir, reducing the temperature gradient in the wide epilimnion and metalimnion, decreasing the dispersion degree of the temperature and the thermal stability. These circumstances are reversed in winter. The inflow discharge decreases and vertical mixing reduces in winter, less cold water enters the reservoir and therefore, water temperatures in the epilimnion and metalimnion decrease more slowly. Consequently, the vertical temperature gradient and dispersion degree of the temperature are relatively large (Fig. 6b). Over a whole year, as C_d increases, the annual average thermal stability decreases slightly. Compared with the baseline (8204.1 J m^{-2}), the annual average thermal stability reaches 8140.8 J m^{-2} (−0.77%) and 8078.2 J m^{-2} (−1.53%) when C_d increases by 13% and 26%, respectively.

3.2.4. Released water temperature

The released water temperature is crucial to the downstream ecology of a reservoir. In summer, as C_d increases, more warm water enters the reservoir, significantly increasing the temperature of the reservoir and its released water (Fig. 7). As C_d increases by 13% and 26%, the average released water temperature in summer increases by 0.63 °C and 1.22 °C, respectively. In winter, the changes in the temperature profile and released water temperature are small. In total, the annual average released water temperature increases by 0.20 °C and 0.40 °C when C_d increased by 13% and 26%, respectively. The increases in the released water temperature are larger than those of the reservoir temperature (A1 = 0.05 °C; A2 = 0.09 °C) for two main reasons: 1) the water intake is located at depths of 35–65 m where the temperature increase is much larger compared to the other layers; and 2) as C_d increases, the thermal stability decreases, and water buoyancy decreases, which favors the sinking of warmer water above the intake, and hence the released water temperature rises further.

In addition, as C_d increases, because of the warmer outflow in summer, the yearly mean of the absolute temperature difference between

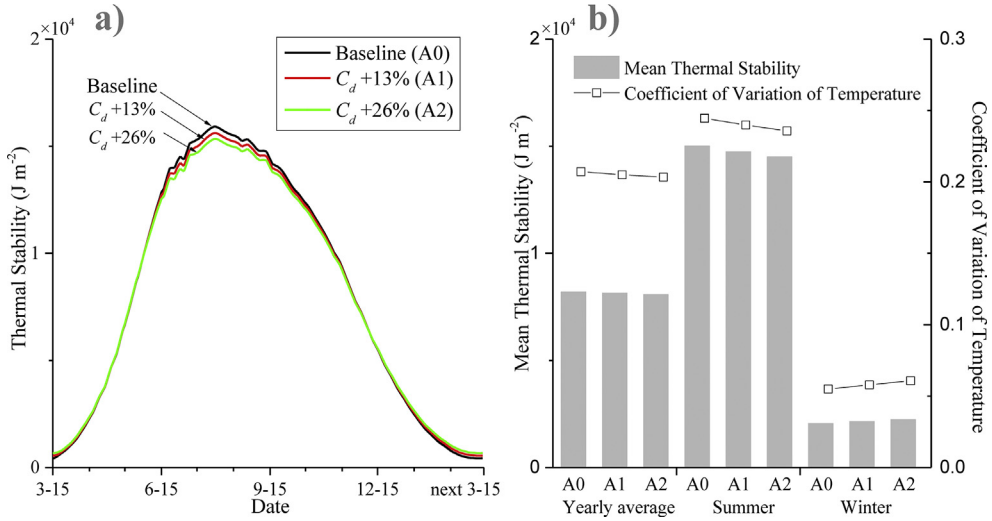

Fig. 6. a) Thermal stability during the year for different intra-annual runoff uniformities; b) comparison of the thermal stability and coefficient of variation of temperature.

inflow runoff and released water (TD) decreases (A0 = 3.55 °C; A1 = 3.39 °C; A2 = 3.24 °C), indicating that a higher C_d helps to mitigate the TD caused by reservoir impoundment.

3.2.5. Sensitivity analysis

The previous section detailed the impact of the intra-annual runoff uniformity on the thermal regime. Next, a sensitivity analysis was performed, and the change in the annual average values was proven to be linearly related to the increase in C_d. As C_d increases by 10%, the annual average values of the reservoir temperature, thermal stability, and released water temperature show changes of 0.036 °C, −48.4 J m^{-2}, and 0.153 °C, respectively.

3.3. Thermal regime in the future

3.3.1. Water temperature

Average reservoir temperature values were calculated considering both the intra-annual runoff uniformity and global warming, as shown in Fig. 8. Owing to the relatively large inflow runoff, and relatively high inflow and air temperatures, the water temperature of the reservoir significantly increases. For the high emission scenario RCP8.5, the volume-weighted average temperature of the whole reservoir increases by 1.57 °C and 2.80 °C (compared with the baseline) by the 2050s and 2090s, respectively. Additionally, the epilimnion is more significantly affected than the hypolimnion.

The main heat inputs of a reservoir are the inflow runoff and air–heat exchange, and increases in the heat input relative to the baseline can be identified (Fig. 9). When C_d is larger, the increase in the heat input comes solely from relatively warm runoff, which predominantly affects the water column at depths of 20–90 m. When intra-annual runoff uniformity and global warming are both considered, the larger inflow runoff and higher inflow and air temperatures significantly increase the heat input and water temperature. In general, global warming has a larger influence on the reservoir temperature than the intra-annual runoff uniformity.

3.3.2. Stratification duration

As global warming elevates the water temperature of the upper layers, the vertical temperature gradient significantly increases, and the stratification durations of all layers increase, except in the hypolimnion. Because the temperature gradient of the hypolimnion is not large enough, a stratification period does not exist. For the high emission scenario RCP8.5, the stratification durations of all layers increase by 7 and 18 days by the 2050s and 2090s, respectively.

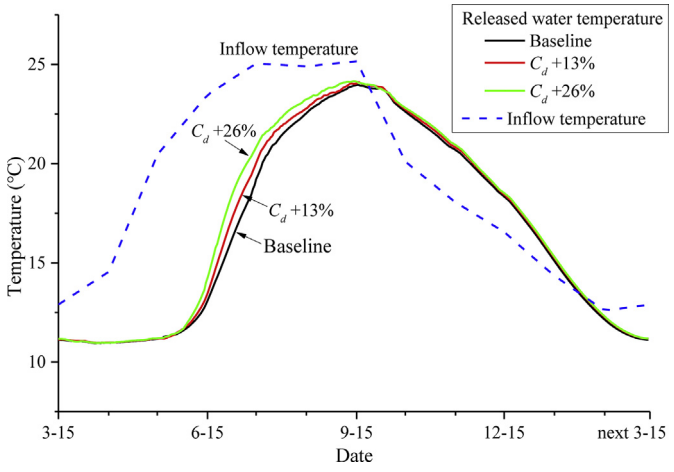

Fig. 7. Released water temperature during one year for different intra-annual runoff uniformities.

3.3.3. Thermal stability

The thermal stabilities under different model scenarios are shown in Fig. 10. Under future climate scenarios, because the increase in water temperature is larger in the epilimnion than in the hypolimnion, the vertical temperature gradient and thermal stability increase. Although a higher C_d reduces the thermal stability, global warming has a much larger impact. In particular, under the high emission scenario RCP8.5, the annual average thermal stability increases by 1062.3 J m^{-2} (+12.9%) and 1939.3 J m^{-2} (+23.6%) by the 2050s and 2090s, respectively.

3.3.4. Released water temperature

A higher C_d and global warming increase the reservoir temperature and furthermore, significantly increase the released water temperature. In particular, under the high emission scenario RCP8.5, the annual average released water temperature could increase by 1.43 °C and 2.65 °C by the 2050s and 2090s, respectively. As the released water temperature increases, the yearly mean TD initially decreases (Fig. 11). However, if the magnitude of global warming is very large, such as in scenario A6 (C_d + 26%&RCP8.5), the TD increases. In general, moderate global warming helps to mitigate the TD caused by reservoir impoundment, but high global warming increases the TD.

3.3.5. Sensitivity analysis

The previous section detailed the influence of global warming on the thermal regime. Next, a sensitivity analysis was performed, and the change in the annual average values was proven to be linearly related to the increase in air temperature. As the air temperature increases by 1 °C, the annual average values of the reservoir temperature, thermal stability, and released water temperature show changes of 0.67 °C, 455 J m^{-2} and 0.60 °C, respectively. By the 2050s and 2090s, even under the medium–low RCP4.5 emission scenario, the impact of global warming on the thermal regime is more significant than that of intra-annual runoff uniformity.

4. Discussion

This study estimated changes in the hydrological conditions in Sanbanxi Reservoir, and showed that the concentration degree of runoff significantly increased during 1950–2015. Previous research has shown that climate change and human activities are the two main factors that can alter a hydrological regime. Sanbanxi Reservoir is located in the upper reaches of the Yuanjiang River, which experiences relatively little human influence. The increased intra-annual uniformity of precipitation in the catchment in recent years is therefore predominantly caused by climate change (Zhang et al., 2007). For the Pearl River Delta and the Dongjiang River in South China, which are not far from the Yuanjiang River, Lin et al. (2017) and Tu et al. (2015) have shown that climate change has increased the concentration degree of the runoff. Wang et al. (2015) showed that the concentration degree of runoff of the Yalong River basin is increasing, especially in the pristine upstream channel. Although changes in intra-annual runoff uniformity are globally unequal (IPCC, 2013), in South China, climate change tends to have a decreasing effect. Conversely, human activities tend to cause decreases in the concentration degree of runoff owing to reservoir regulation, as has been shown for the Yangtze River, the Dongjiang River, the Poyang Lake Basin, the Ili River, and the Pearl River Delta (Gu et al., 2016; Guo et al., 2015; Lin et al., 2017; Tu et al., 2015; Zhao et al., 2012). Overall, for South China, climate change tends to increase the C_d of runoff, and human activities tend to decrease the C_d of runoff. The C_d of pristine rivers such as those feeding the Sanbanxi Reservoir tends to increase, and for rivers which are significantly affected by human activities, C_d tends to decrease.

Here, the impact of intra-annual runoff uniformity on the thermal regime of Sanbanxi Reservoir and its impact on other reservoirs were also investigated. For a reservoir, as C_d increases, the warm runoff in

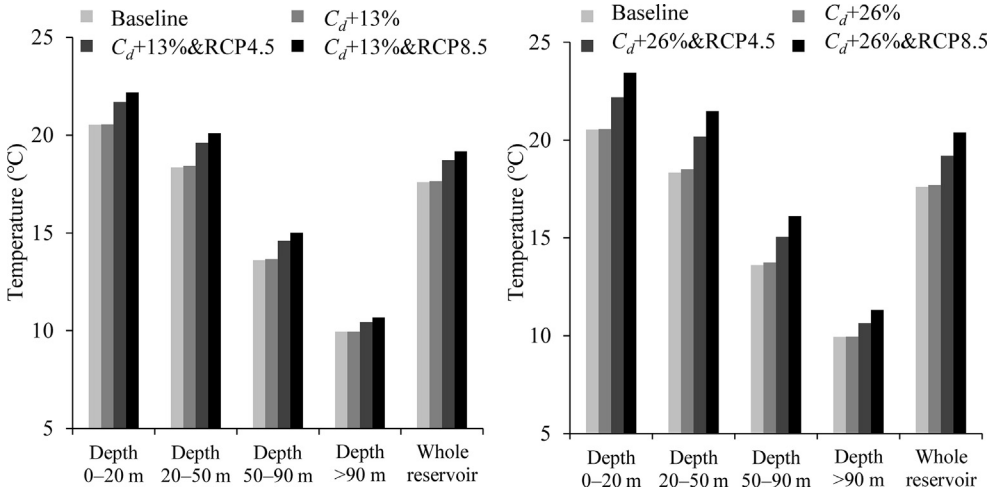

Fig. 8. Reservoir temperatures for different climate scenarios.

summer increases and the cold runoff in winter decreases, and hence the reservoir and released water temperatures increase. In the flood season, when thermal stratification is relatively strong, relatively large runoff amounts increase the vertical mixing of the water column. Moreover, more warm water reduces the temperature gradient in the wide epilimnion and metalimnion, decreasing thermal stability; the opposite scenario occurs in winter. Owing to the relatively weak stratification and small water volume in winter, the increase in thermal stability is smaller than that occurring in summer. As a result, the annual average of the thermal stability is smaller for larger values of C_d. In general, a higher C_d increases the annual average values of the reservoir and released water temperatures, and decreases that of thermal stability. These changes are applicable to other reservoirs besides Sanbanxi Reservoir.

For Sanbanxi Reservoir, global warming is increasing the annual average temperature of the reservoir, the released water temperatures, and the stratification duration, which accords with the results of Modiri-Gharehveran et al. (2014), Zhang et al. (2015), and Prats et al. (2018). Moreover, this paper shows that global warming will increase thermal stability. Firstly, for the reservoir area, increases in thermal stability and the stratification duration will facilitate oxygen stratification and cause hypolimnetic anoxia, deteriorating water quality. Furthermore, the increase in the water temperature will promote algae growth and even aggravate algae bloom occurrence (Gu et al., 2016; Guo et al., 2015; Lin et al., 2017; Tu et al., 2015; Zhao et al., 2012), especially in eutrophic reservoirs such as Sanbanxi Reservoir (Ou et al., 2014). Secondly, the released water temperature is significantly different from the natural inflow temperature, and the TD is modelled to reach 3.00 °C by the 2090s (scenario A5: C_d + 26%&RCP4.5). The cold outflow will delay fish spawning, particularly in spring and summer, which are the main spawning periods for fish in Southwest China (He et al., 2018). For example, before the impoundment of Sanbanxi Reservoir, the four major species of Chinese carp, whose minimum spawning temperature is ~18 °C (Wang et al., 2014), began to spawn around March 1st. By the 2090s (scenario A5: C_d + 26%&RCP4.5), this date is expected to be June 20th.

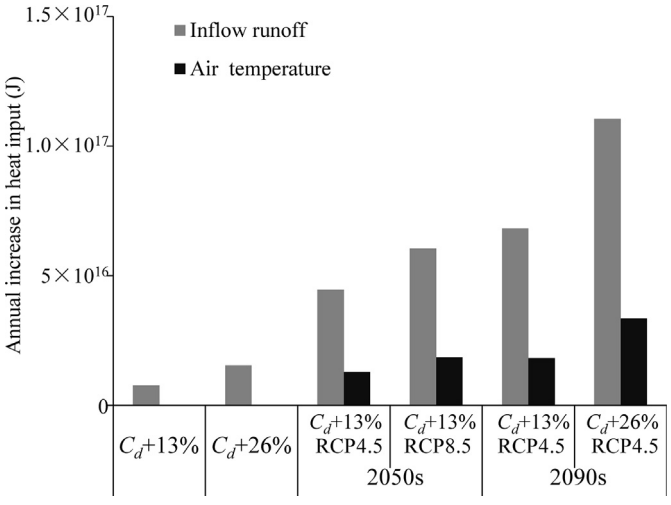

Fig. 9. Annual increase in the heat input from inflow runoff and air–heat exchange.

Two control methods are considered to decrease thermal stability and the TD, including changing the reservoir operation level and changing the intake elevation. Taking scenario A5 as an example, the effects of implementing these control methods are shown in Table 4. Overall, a relatively high reservoir operation level or a relatively low intake elevation will reduce thermal stability and increase the TD, and vice versa. Through sensitivity analysis, the effect of changing the intake elevation is shown to be more significant than that of changing the reservoir operation level. Selective withdrawal is not only effective in controlling the released water temperature (Rheinheimer et al., 2015), but also in changing the reservoir's thermal stability. Additionally, changes in the reservoir operation level or intake elevation will influence the power head and economic benefit of the reservoir and the structural safety of the hydraulic engineering infrastructure. In practice, determination of the appropriate control method should comprehensively consider the multi-dimensional (e.g., ecological benefit, economic benefit, and structural safety) and multi-domain (e.g., the reservoir area and downstream) effects on the reservoir.

As C_d increases, the extreme floods with high solid content may occur more frequently in the reservoir, and their influence was investigated. This paper shows that the increased inflow runoff in summer decreases the thermal stability; hence the extreme flood will significantly promote the vertical mixing, which is also proved by Huang et al. (2014) and Liu et al. (2011). Moreover, the increased high solid content will further increase the water density of inflow and intensify the density current at the reservoir tail, and promote the vertical mixing of stratified (Ma et al., 2015; Yu and Wang, 2011). In general, the extreme flood with high solid will significantly disturb the thermal stratification, and expand the influence of intra-annual runoff uniformity on the thermal regime.

There are some limitations, however. Firstly, the long-term pattern of hydrological conditions and global warming are very complex and may be related. The hydrological mechanisms under climate change can be further studied, and a more accurate prediction method for C_d should be developed. Secondly, according to the IPCC (2013), besides

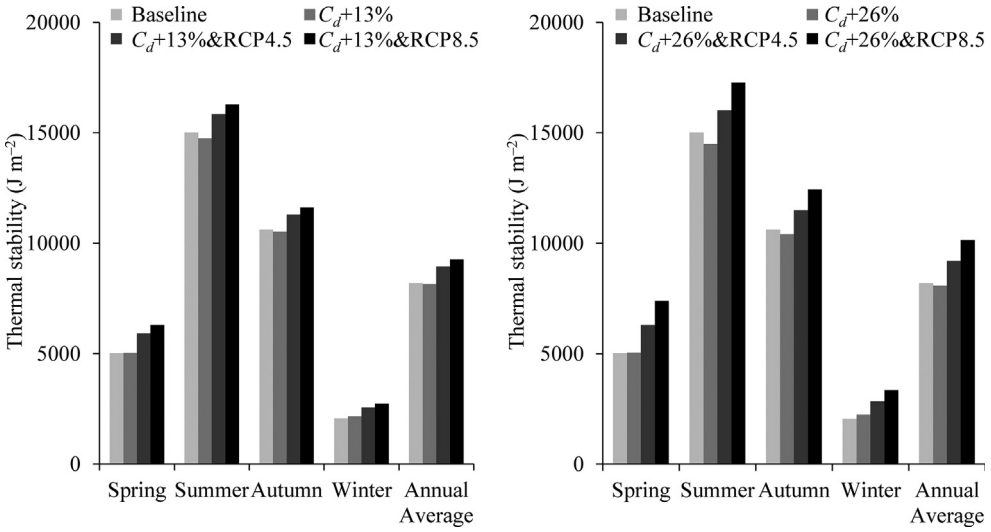

Fig. 10. Thermal stability under different climate scenarios.

runoff and temperature, which are two sensitive factors affecting thermal regime, other variables such as wind, solar radiation, and precipitation may also change in many regions, and the impact of these factors on the thermal regimes requires further research. Thirdly, the monthly mean values of wind speed were adopted here to setup the model scenarios. Sudden large wind events were ignored. Such events should be considered as they may substantially promote water column mixing and, thus, influence thermal regimes (Saber et al., 2018).

5. Conclusions

Thermal regime has a great influence on the aquatic environment and ecology of reservoir basins. This study statistically analyzed trends of intra-annual runoff uniformity for Sanbanxi Reservoir over the past 66 years, examined the associated impacts on the reservoir's thermal regime, and evaluated the thermal regime under future climate scenarios. The following conclusions can be drawn from this research:

1) For South China, the C_d of pristine rivers tends to be higher and, for rivers significantly impacted by human activities, C_d tends to be lower. For the Sanbanxi Reservoir basin, which is relatively unaffected by human activity, C_d shows a significant increasing trend over recent decades and is predicted to increase by approximately 13% and 26% by the 2050s and 2090s, respectively.
2) A higher C_d elevates the reservoir and released water temperatures, and decreases thermal stability, and its influence is larger in summer than in other seasons. For Sanbanxi Reservoir, a C_d increase of 10% results in a change in annual average reservoir temperature, thermal stability, and released water temperature of 0.036 °C, −48.4 J m^{-2}, and 0.153 °C, respectively.
3) Global warming increases the reservoir temperature, released water temperature and thermal stability, and its influence is larger than that of intra-annual runoff uniformity in Sanbanxi Reservoir. If air temperature increases by 1 °C, annual average values of reservoir temperature, thermal stability, and released water temperature are predicted to increase by 0.67 °C, 455 J m^{-2}, and 0.60 °C, respectively.
4) The predicted future increase in thermal stability may intensify oxygen stratification and hypolimnetic anoxia. The increased water temperature will likely promote algae blooms, and the colder outflow may delay fish spawning in spring and summer. In particular, the date of spawning for four major species of Chinese carp is predicated to be delayed from around March 1st (prior to reservoir impoundment) to June 20th in the 2090s.
5) The effects of two control methods on the reservoir's thermal regime were analyzed. When the reservoir operation level is increased or the intake elevation is reduced, thermal stability is reduced and the TD is increased, and vice versa. The effect of changing the intake elevation is more significant than that of changing the reservoir operation level.

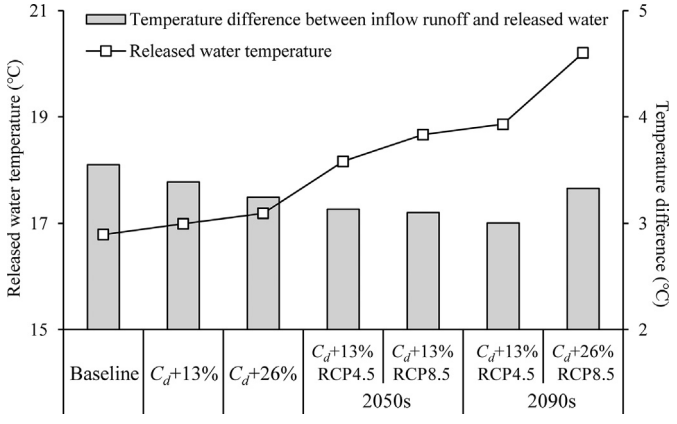

Fig. 11. Annual average released water temperature and the temperature difference between inflow runoff and released water for different climate scenarios.

In this study, variations in the thermal regime of a large reservoir under climate change were investigated. Reservoir basin temperature

Table 4
Effects of implementing different control methods.

Scenarios		Thermal stability (J m^{-2})	TD (°C)
A5		9194.2	3.00
Reservoir operation level (m)	−5[a]	9294.0	2.77
	−2.5	9225.7	2.88
	2.5	9038.9	3.13
	5	8953.9	3.30
Intake elevation (m)	−20	5574.8	3.53
	−10	8160.6	3.40
	10	9883.0	2.85
	20	10,230.2	2.34

[a] A positive (negative) number indicates the ascent (descent) of the water level or intake elevation.

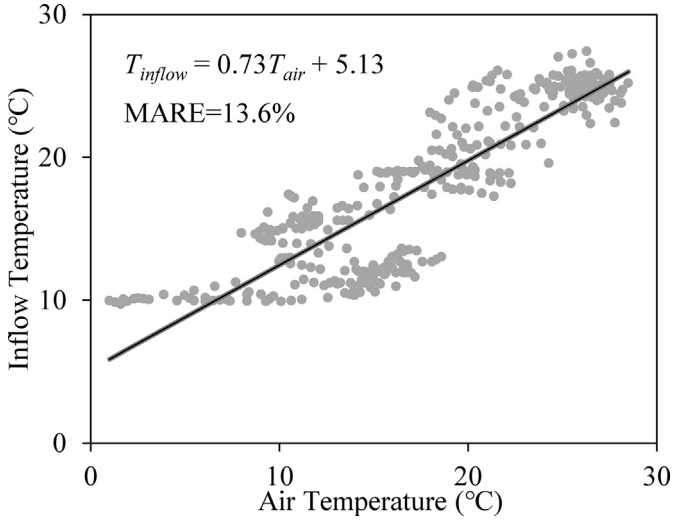

Fig. 12. Relationship between the air and inflow temperatures.

management in the future should be adjusted considering the results of this research,

Acknowledgements

This research was supported by the National Key R&D Program of China (Nos. 2016YFC0401810 and 2016YFC0401702), the Fundamental Research Funds for the Central Universities (2019B11114) and the National Natural Science Foundation of China (Nos. 51479010, 51779016 and 51839008). The authors thank Dr. Thomas Cole, United States Army Corps of Engineers and Dr. Scott Wells, Portland State University for the source code of CE-QUAL-W2 (http://www.ce.pdx.edu/w2/), and the anonymous reviewers for their helpful suggestions.

Appendix A*A.1.* *Nomenclature*

C_d	concentration degree
C_p	concentration period
H_0	null hypothesis
IPCC	Intergovernmental Panel on Climate Change
MAE	mean absolute error
MARE	mean absolute relative error
MK test	Mann-Kendall test
$\overline{q}$	annual average inflow
r_1	lag-1 serial correlation of the time series
RCP	Representative Concentration Pathway
RMSE	root mean square error
T_{air}	air temperature
T_{inflow}	inflow temperature
TD	temperature difference between inflow runoff and released water
UF_k	the normalized statistic index of the MK test
β	Theil-Sen estimator

A.2. Basic equations for the CE-QUAL-W2 model

A.2.1. Continuity equation

$$\frac{\partial UB}{\partial x} + \frac{\partial WB}{\partial z} qB \tag{A.1}$$

A.2.2. x-momentum equation

$$\begin{aligned}&\frac{\partial UB}{\partial t} + \frac{\partial UUB}{\partial x} + \frac{\partial WUB}{\partial z} = gB\ \sin\alpha + gB\ \cos\alpha \frac{\partial \eta}{\partial x} \\ &-\frac{gB\ \cos\alpha}{\rho}\int_{\eta}^{z} \frac{\partial \rho}{\partial x} dz + \frac{1}{\rho}\frac{\partial B\tau_{xx}}{\partial x} + \frac{1}{\rho}\frac{\partial B\tau_{xz}}{\partial z} + qBU_x\end{aligned} \tag{A.2}$$

A.2.3. z-momentum equation

$$0 = g\ \cos\alpha - \frac{1}{\rho}\frac{\partial P}{\partial z} \tag{A.3}$$

A.2.4. Free surface equation

$$B_n \frac{\partial \eta}{\partial t} = \frac{\partial}{\partial x}\int_{\eta}^{h} UBdz - \int_{\eta}^{h} qBdz \tag{A.4}$$

A.2.5. State equation

$$\rho = f\left(T^w, \Phi_{TDS}, \Phi_{ISS}\right) \tag{A.5}$$

A.2.6. Heat-balance equation

$$\frac{\partial B\Phi}{\partial t} + \frac{\partial UB\Phi}{\partial x} + \frac{\partial WB\Phi}{\partial z} - \frac{\partial\left(BD_x \frac{\partial \Phi}{\partial x}\right)}{\partial x} - \frac{\partial\left(BD_z \frac{\partial \Phi}{\partial z}\right)}{\partial z} = q_\Phi B + S_\Phi B \tag{A.6}$$

A.2.7. Vertical shear stress

$$\frac{\tau_{xz}}{\rho} = A_z \frac{\partial V}{\partial z} \tag{A.7}$$

$$A_z = \kappa\left(\frac{{l_m}^2}{2}\right)\sqrt{\left(\frac{\partial U}{\partial z}\right)^2 + \left(\frac{\tau_{wy}e^{-2kz} + \tau_{y-tributary}}{\rho\nu_t}\right)^2}\, e^{(-CR_i)} \tag{A.8}$$

$$l_m = \Delta z_{\max} \tag{A.9}$$

$$R_i = \frac{g\frac{\partial \rho}{\partial z}}{\rho\left(\frac{\partial U}{\partial z}\right)^2} \tag{A.10}$$

A.2.8. Surface heat exchange

$$H_n = H_s + H_a + H_e + H_c - (H_{sr} + H_{ar} + H_{br}) \tag{A.11}$$

where, U and W are the x- and z-direction velocities, respectively (m s^{-1}); B is the control volume width (m); q is the net lateral inflow of a constituent per unit volume (s^{-1}); a is the channel slope (rad); g is the gravitational acceleration (m s^{-2}); τ is the shear stress (N m^{-2}); ρ is the water density (m^3 s^{-1}); η is the free surface elevation (m); P is the pressure (Pa); and f is the density function, which is dependent upon temperature T_w, total dissolved solids or salinity Φ_{TDS}, and

inorganic suspended solids Φ_{ISS}. Because the amounts of total dissolved and inorganics suspended solids in the Sanbanxi Reservoir are small, and the salinity is 0, only temperature is considered to affect the density. Φ is the lateral-averaged thermal concentration ($J\,m^{-3}$); D_x and D_z are the longitudinal and vertical temperature dispersion coefficients, respectively ($m\,s^{-2}$); q_Φ is the lateral inflow of a constituent per unit volume ($J{\cdot}m^{-3}\,s^{-1}$);S_Φ is the kinetic source/sink term for a constituent concentration ($J{\cdot}m^{-3}\,s^{-1}$); κ is the von Karman constant of 0.4; l_m is the mixing length (m); τ_{wy} is the cross-shear from wind ($N\,m^{-2}$); R_i is the Richardson number; k is the wave number, C is a constant and is assumed to be 0.15; Δz_{max} is the maximum vertical grid spacing (m); H_n is the net rate of heat exchange across the water surface ($W\,m^{-2}$); H_s is the incident short-wave solar radiation ($W\,m^{-2}$); H_a is the incident long-wave radiation ($W\,m^{-2}$); H_e is the evaporative heat loss ($W\,m^{-2}$); H_c is the heat conduction ($W\,m^{-2}$); H_{sr} is the reflected short-wave solar radiation ($W\,m^{-2}$); H_{ar} is the reflected long-wave radiation ($W\,m^{-2}$); and H_{br} is the back radiation from the water surface ($W\,m^{-2}$).

A.3. Relationship of air and inflow temperatures

The increase in the inflow temperature under the future scenarios was derived from daily air and inflow temperature data between June 2015 to March 2016. The relationship between the air and inflow temperatures in Sanbanxi Reservoir can be approximated by the formula $T_{inflow} = 0.73T_{air} + 5.13$. The linear correlation coefficient and MARE are 0.87 and 13.6%, respectively (Fig. 12). In addition, the inflow discharge may influence the runoff temperature, and a correlation analysis between these two variables was conducted. The linear correlation coefficient is 0.16, indicating a weak linear correlation. For simplicity, the inflow temperature was considered to be a linear function of air temperature.

References

Anohin, V.V., Imberger, J., Asce, M., Romero, J.R., Ivey, G.N., 2006. Effect of long internal waves on the quality of water withdrawn from a stratified reservoir. J. Hydraul. Eng. 132 (11), 1134–1145.

Assani, A.A., Quessy, J., Mesfioui, M., Matteau, M., 2010. An example of application: the ecological "natural flow regime" paradigm in hydroclimatology. Adv. Water Resour. 33 (5), 537–545. https://doi.org/10.1016/j.advwatres.2010.02.005.

Bocchiola, D., 2014. Long term (1921–2011) hydrological regime of Alpine catchments in Northern Italy. Adv. Water Resour. 70, 51–64. https://doi.org/10.1016/j.advwatres.2014.04.017.

Butcher, J.B., Nover, D., Johnson, T.E., Clark, C.M., 2015. Sensitivity of lake thermal and mixing dynamics to climate change. Clim. Chang. 129 (1–2), 295–305. https://doi.org/10.1007/s10584-015-1326-1.

Cole, T.M., Wells, S.A., 2015. CE-QUAL-W2: A Two-Dimensional, Laterally Averaged, Hydrodynamic and Water Quality Model, Version 3.72 User Manual. Department of Civil and Environmental Engineering, Portland State University, Portland, OR.

Elçi, Ş., 2008. Effects of thermal stratification and mixing on reservoir water quality. Limnology 9 (2), 135–142. https://doi.org/10.1007/s10201-008-0240-x.

Gu, C., Mu, X., Zhao, G., Gao, P., Sun, W., Yu, Q., 2016. Changes in stream flow and their relationships with climatic variations and anthropogenic activities in the Poyang Lake Basin, China. Water-Sui. 8 (12), 564. https://doi.org/10.3390/w8120564.

Guo, L., Xia, Z., Zhou, H., Huang, F., Yan, B., 2015. Hydrological changes of the Ili River in Kazakhstan and the possible causes. J. Hydrol. Eng. 20 (0501500611). https://doi.org/10.1061/(ASCE)HE.1943-5584.0001214.

Han, B., Armengol, J., Carlos Garcia, J., Comerma, M., Roura, M., Dolz, J., Straskraba, M., 2000. The thermal structure of Sau reservoir (NE: Spain): a simulation approach. Ecol. Model. 125 (2–3), 109–122. https://doi.org/10.1016/S0304-3800(99)00176-3.

He, W., Lian, J., Du, H., Ma, C., 2018. Source tracking and temperature prediction of discharged water in a deep reservoir based on a 3-D hydro-thermal-tracer model. J. Hydro Environ. Res. 20, 9–21. https://doi.org/10.1016/j.jher.2018.04.002.

Hetherington, A.L., Schneider, R.L., Rudstam, L.G., Gal, G., DeGaetano, A.T., Walter, M.T., 2015. Modeling climate change impacts on the thermal dynamics of polymictic Oneida Lake, New York, United States. Ecol. Model. 300, 1–11. https://doi.org/10.1016/j.ecolmodel.2014.12.018.

Huang, T., Li, X., Rijnaarts, H., Grotenhuis, T., Ma, W., Sun, X., Xu, J., 2014. Effects of storm runoff on the thermal regime and water quality of a deep, stratified reservoir in a temperate monsoon zone, in Northwest China. Sci. Total Environ. 485–486, 820–827. https://doi.org/10.1016/j.scitotenv.2014.01.008.

IPCC, 2013. Climate change 2013: The Physical Science Basis (10 pp).

Lee, H.W., Kim, E.J., Park, S.S., Choi, J.H., 2012. Effects of climate change on the thermal structure of lakes in the Asian Monsoon Area. Clim. Chang. 112 (3–4), 859–880. https://doi.org/10.1007/s10584-011-0233-3.

Li, X., Jiang, F., Li, L., Wang, G., 2010. Spatial and temporal variability of precipitation concentration index, concentration degree and concentration period in Xinjiang, China. Int. J. Climatol., 1679–1693 https://doi.org/10.1002/joc.2181.

Li, F., Zhang, G., Xu, Y.J., 2014. Spatiotemporal variability of climate and streamflow in the Songhua River Basin, Northeast China. J. Hydrol. 514, 53–64. https://doi.org/10.1016/j.jhydrol.2014.04.010.

Lian, J., Yao, Y., Ma, C., Guo, Q., 2014. Reservoir operation rules for controlling algal blooms in a tributary to the impoundment of three gorges dam. Water-Sui. 6 (10), 3200–3223. https://doi.org/10.3390/w6103200.

Lian, J., He, W., Ma, C., Xu, K., 2015. Guarantee rate of freshwater in a river mouth intruded by saltwater with respect to the joint impact of runoff and tide. J. Hydroinf. 17 (6), 917–929. https://doi.org/10.2166/hydro.2015.038.

Lin, K., Lin, Y., Xu, Y., Chen, X., Chen, L., Singh, V.P., 2017. Inter- and intra- annual environmental flow alteration and its implication in the Pearl River Delta, South China. J. Hydro Environ. Res. 15, 27–40. https://doi.org/10.1016/j.jher.2017.01.002.

Liu, W., Jiang, D., Cheng, T., 2011. Effects of flood on thermal structure of a stratified reservoir. Procedia Environ. Sci. 10, 1811–1817. https://doi.org/10.1016/j.proenv.2011.09.283.

Luce, C.H., Holden, Z.A., 2009. Declining annual streamflow distributions in the Pacific Northwest United States, 1948–2006. Geophys. Res. Lett. 36 (16). https://doi.org/10.1029/2009GL039407.

Ma, J., Liu, D., Wells, S.A., Tang, H., Ji, D., Yang, Z., 2015. Modeling density currents in a typical tributary of the Three Gorges Reservoir, China. Ecol. Model. 296, 113–125. https://doi.org/10.1016/j.ecolmodel.2014.10.030.

Milstein, A., Zoran, M., 2001. Effect of water withdrawal from the epilimnion on thermal stratification in deep dual purpose reservoirs for fish culture and field irrigation. Aquac. Int. 9 (1), 81–86. https://doi.org/10.1023/A:1012530409312.

Modiri-Gharehveran, M., Jabbari, E., Etemad-Shahidi, A., 2014. Effects of climate change on the thermal regime of a reservoir. Proc. Inst. Civ. Eng. Water Manage. 167 (10), 601–611. https://doi.org/10.1680/wama.12.00124.

Moriasi, D.N., Arnold, J.G., Van Liew, M.W., Bingner, R.L., Harmel, R.D., Veith, T.L., 2007. Model evaluation guidelines for systematic quantification of accuracy in watershed simulations. Trans. ASABE 50 (3), 885–900.

Ou, T., Li, Q., Wang, A., Zhang, L., Huang, G., Jiao, S., Gao, T., 2014. The correlation between dynamic change of phytoplankton community structure and environmental factors in Sanbanxi Reservoir of Guizhou Plateau. Chin. J. Eco. 12 (33), 3432–3439 (in Chinese).

Petersen, T., Devineni, N., Sankarasubramanian, A., 2012. Seasonality of monthly runoff over the continental United States: causality and relations to mean annual and mean monthly distributions of moisture and energy. J. Hydrol. 468–469, 139–150. https://doi.org/10.1016/j.jhydrol.2012.08.028.

Prats, J., Salençon, M., Gant, M., Danis, P., 2018. Simulation of the hydrodynamic behaviour of a Mediterranean reservoir under different climate change and management scenarios. J. Limnol. 77 (1). https://doi.org/10.4081/jlimnol.2017.1567.

Rheinheimer, D.E., Null, S.E., Lund, J.R., 2015. Optimizing selective withdrawal from reservoirs to manage downstream temperatures with climate warming. J. Water Resour. Plan. Manag. 141 (4), 4014063. https://doi.org/10.1061/(ASCE)WR.1943-5452.0000447.

Saber, A., James, D.E., Hayes, D.F., 2018. Effects of seasonal fluctuations of surface heat flux and wind stress on mixing and vertical diffusivity of water column in deep lakes. Adv. Water Resour. 119, 150–163. https://doi.org/10.1016/j.advwatres.2018.07.006.

Soleimani, S., Bozorg-Haddad, O., Saadatpour, M., Loaiciga, H.A., 2016. Optimal selective withdrawal rules using a coupled data mining model and genetic algorithm. J. Water Res. Plan. Man. 142, 0401606412. https://doi.org/10.1061/(ASCE)WR.1943-5452.0000717.

Stahl, K., Hisdal, H., Hannaford, J., Tallaksen, L.M., van Lanen, H.A.J., Sauquet, E., Demuth, S., Fendekova, M., Jódar, J., 2010. Streamflow trends in Europe: evidence from a dataset of near-natural catchments. Hydrol. Earth Syst. Sci. 14 (12), 2367–2382. https://doi.org/10.5194/hess-14-2367-2010.

Sun, S., Barraud, S., Castebrunet, H., Aubin, J., Marmonier, P., 2015. Long-term stormwater quantity and quality analysis using continuous measurements in a French urban catchment. Water Res. 85, 432–442. https://doi.org/10.1016/j.watres.2015.08.054.

Tu, X., Singh, V.P., Chen, X., Chen, L., Zhang, Q., Zhao, Y., 2015. Intra-annual distribution of streamflow and individual impacts of climate change and human activities in the Dongijang river basin, China. Water Resour. Manag. 29 (8), 2677–2695. https://doi.org/10.1007/s11269-015-0963-5.

Wang, S., Qian, X., Han, B., Luo, L., Hamilton, D.P., 2012. Effects of local climate and hydrological conditions on the thermal regime of a reservoir at tropic of Cancer, in southern China. Water Res. 46 (8), 2591–2604. https://doi.org/10.1016/j.watres.2012.02.014.

Wang, J.N., Li, C., Duan, X.B., Luo, H.H., Feng, S.X., Peng, Q.D., Liao, W.G., 2014. The relationship between thermal regime alteration and spawning delay of the four major Chinese carps in the Yangtze river below the three gorges dam. River Res. Appl. 30 (8), 987–1001. https://doi.org/10.1002/rra.2691.

Wang, B., Wang, L., Li, C., Ma, Y., Chen, F., 2015. Research on the Runoff's distribution characteristics of the Year in the Yalong River. China Rural Water Hydr. 11, 81–84 (in Chinese).

Wu, B., Wang, G., Jiang, H., Wang, J., Liu, C., 2016. Impact of revised thermal stability on pollutant transport time in a deep reservoir. J. Hydrol. 535, 671–687. https://doi.org/10.1016/j.jhydrol.2016.02.031.

Xie, Z., Du, Y., Jiang, A., Ding, Y., 2005. Climatic trends of different intensity heavy precipitation events concentration in China. J. Geogr. Sci. 15 (4), 459–466. https://doi.org/10.1360/gs050409.

Xie, P., Xu, B., Hu, C., Chen, G., Liu, X., Tang, Y., 2011. Alteration of inner-annual runoff distribution and attribution analysis of Longchuan station at Dongjiang River. IEEE: International Symposium on Water Resource & Environmental Protection. IEEE, pp. 572–575 https://doi.org/10.1109/ISWREP.2011.5893071 edited.

Xu, J., Chen, Y., Li, W., Dong, S., 2008. Long-term trend and fractal of annual runoff process in mainstream of Tarim River. Chin. Geogr. Sci. 18 (1), 77–84. https://doi.org/10.1007/s11769-008-0077-6.

Yang, X., Huang, T., Zhang, H., 2015. Effects of seasonal thermal stratification on the functional diversity and composition of the microbial community in a drinking water reservoir. Water-Sui. 7 (10), 5525–5546. https://doi.org/10.3390/w7105525.

Yu, Z., Wang, L., 2011. Factors influencing thermal structure in a tributary bay of three gorges reservoir. J. Hydrodyn. 04, 407–415.

Zhang, L., Qian, Y., 2003. Annual distribution features of precipitation in China and their interannual variations. Acta Metall. Sin. 02, 146–163.

Zhang, Z., Chen, X., Wang, W., Shi, P., 2007. Analysis of rainfall trend and extreme events in Guizhou. Earth Environ. 35 (4), 351–356 (in Chinese).

Zhang, Y., Guan, D., Jin, C., Wang, A., Wu, J., Yuan, F., 2011. Analysis of impacts of climate variability and human activity on streamflow for a river basin in northeast China. J. Hydrol. 410 (3–4), 239–247. https://doi.org/10.1016/j.jhydrol.2011.09.023.

Zhang, Y., Wu, Z., Liu, M., He, J., Shi, K., Zhou, Y., Wang, M., Liu, X., 2015. Dissolved oxygen stratification and response to thermal structure and long-term climate change in a large and deep subtropical reservoir (Lake Qiandaohu, China). Water Res. 75, 249–258. https://doi.org/10.1016/j.watres.2015.02.052.

Zhao, J., Li, J., Dai, Z., Wang, Y., Zhang, A., 2012. Analysis the runoff variation of Yangtze River in Yichang. Resources Science 12, 2306–2315 (in Chinese).

Zhu, K., Bi, Y., Hu, Z., 2013. Responses of phytoplankton functional groups to the hydrologic regime in the Daning River, a tributary of Three Gorges Reservoir, China. Sci. Total Environ. 450–451, 169–177. https://doi.org/10.1016/j.scitotenv.2013.01.101.

Zouabi-Aloui, B., Adelana, S.M., Gueddari, M., 2015. Effects of selective withdrawal on hydrodynamics and water quality of a thermally stratified reservoir in the southern side of the Mediterranean Sea: a simulation approach. Environ. Monit. Assess. 187 (5). https://doi.org/10.1007/s10661-015-4509-3.